

Analytic expression for Taylor–Couette stability boundary

Alexander Esser and Siegfried Grossmann

Fachbereich Physik der Philipps-Universität, Renthof 6, D-35032, Marburg, Germany
(July 17, 2018)

We analyze the mechanism that determines the boundary of stability in Taylor–Couette flow. By simple physical argument we derive an analytic expression to approximate the stability line for all radius ratios and all speed ratios, for co- and counterrotating cylinders. The expression includes viscosity and so generalizes Rayleigh’s criterion. We achieve agreement with linear stability theory and with experiments in the whole parameter space. Explicit formulae are given for limiting cases.

PACS 47.15.Fe, 47.20.Gv

1. Introduction

The Taylor–Couette system has been studied for more than 100 years, beginning with the first experiments by Couette [1], Mallock [2], and the pioneering work by Taylor [3]; for a recent review see Tagg [4].

We here focus on the question when and why the laminar flow becomes unstable. This can and has been evaluated with linear stability theory [3,5–9], and was measured for a variety of radius ratios [3,10–13]. The aim of this note is to elucidate the physical mechanism and derive a simple approximate analytical formula for the stability boundary in the whole parameter space.

Earlier attempts of this kind have been made by Donnelly and Fultz [10], Coles [14], Joseph [7], and Eckhardt and Yao [15]. However, these authors did not consider all relevant aspects. Those include the smooth crossover from a solid boundary (for corotation) to a free one (for sufficiently strong counterrotation) and the localization of the initial perturbation in the center of the relevant gap. We elaborate that in Sects. 2–4.

We consider an incompressible fluid with kinematic viscosity ν flowing between two concentric cylinders with inner radius r_1 and outer radius r_2 , and angular velocities $\omega_1 > 0$ and ω_2 , positive for corotation and negative for counterrotation. This fluid flow is characterized by the Reynolds numbers $R_i = \omega_i r_i d / \nu$ ($i = 1, 2$), where $d = r_2 - r_1$ is the gap size between the cylinders.

The well-known [5,16] laminar flow is purely azimuthal and has the velocity profile

$$u_\varphi(r) = Ar + \frac{B}{r} \quad \text{with} \quad (1)$$

$$A = -\frac{\eta^2 \omega_1 - \omega_2}{1 - \eta^2}, \quad B = \frac{\omega_1 - \omega_2}{1 - \eta^2} r_1^2.$$

The radius ratio $\eta = r_1/r_2$ characterizes the geometry of the system. For counterrotation a nodal surface exists where $u_\varphi = 0$,

$$r_n = r_2 \sqrt{\frac{R_1 - \eta R_2}{R_1 - \eta^{-1} R_2}}, \quad R_2 \leq 0. \quad (2)$$

2. Derivation of the stability criterion

Let us start with Rayleigh’s stability argument for inviscid flow [17]: Consider two neighbouring fluid rings at r and $r + \delta r$ of the laminar flow. Stability is guaranteed if their hypothetical exchange by virtual motion through the surrounding flow costs kinetic energy. Neglecting momentum loss by viscosity, the angular momenta per mass $L(r) = r u_\varphi(r)$ of the rings are conserved, and with their kinetic energy per mass being $u_\varphi^2/2$ we arrive at Rayleigh’s famous stability criterion $L^2(r)' > 0$ when considering the energy balance

$$-\delta E_{\text{kin}} = \frac{1}{2} \left(\frac{L(r + \delta r)}{r} \right)^2 - \frac{1}{2} \left(\frac{L(r + \delta r)}{r + \delta r} \right)^2$$

$$+ \frac{1}{2} \left(\frac{L(r)}{r + \delta r} \right)^2 - \frac{1}{2} \left(\frac{L(r)}{r} \right)^2 = \frac{L^2(r)'}{r^3} (\delta r)^2 > 0.$$

δr has been chosen infinitesimal and the prime denotes the r -derivative. Stability is predicted for corotation if $R_1 < R_2/\eta$, and in the case of counterrotation for $R_1 = 0$ only.

Now we take into account viscosity. During the motion to exchange the two fluid rings as described above they lose angular momentum and thus kinetic energy by dissipation. The frictional energy loss per mass is given by the viscous force per mass times the shift δr ,

$$\delta E_{\text{vis}} \sim \left(\frac{\nu}{\ell^2} \delta u_r \right) \delta r.$$

ℓ denotes the typical diameter of the ring (in radial as well as in axial direction). $\delta u_r = \delta r / \delta t$ is the radial velocity of the shift which takes place within time δt . The ‘ \sim ’ symbol means ‘up to a factor of order unity’. For instability, δE_{kin} has to exceed δE_{vis} . Its lower limit is related to the upper limit for δt , which is set by the diffusive time scale, on which the rings lose angular momentum, $\delta t \sim \ell^2 / \nu$. We now obtain from $\delta E_{\text{kin}} \sim \delta E_{\text{vis}}$

$$-\frac{L^2(r)'}{r^3} (\delta r)^2 \sim \frac{\nu^2}{\ell^4} (\delta r)^2 \quad (3)$$

as a relation which characterizes the stability boundary, or, after inserting the profil (1), i.e., $L = Ar^2 + B$,

$$\left[\frac{2}{1+\eta} (\eta R_1 - R_2) \right]^2 \left[\frac{r_n^2}{r^2} - 1 \right] \sim \left(\frac{d}{\ell} \right)^4. \quad (4)$$

Here $r_n^2 = -B/A$, which for negative R_2 coincides with the squared position of the nodal surface.

In contrast to the inviscid case the timescale for the motion and the size of the rings enter here; the expression on the rhs. of (3) has also been used in [14]. As we will see soon, the radial position of the rings is important as well.

ℓ is some small but finite fraction of the part of the gap which is susceptible to instability. For positive R_2 this is the whole gap between the cylinders, therefore we write $\ell = \alpha d$ with α a constant considerably smaller than 1 [14]. We shall determine it by comparison with linear stability analysis.

In the counterrotating case $L^2(r)$ decreases in the range from the inner cylinder up to the nodal surface only. We therefore compare ℓ with $d_n = r_n - r_1$, which is an old idea, cf also [10]. We further take into account that the flow patterns appearing at the instability line extend beyond the nodal surface [3]. This may be understood as a change in the type of boundary from solid (for $R_2 \geq 0$) to sort of free (for $R_2 < 0$). The simplest way of describing this crossover is

$$\ell = \alpha d \Delta(a \frac{d_n}{d}) \quad \text{with} \quad \Delta(x) = \begin{cases} x & , \text{ if } x < 1 \\ 1 & , \text{ if } x \geq 1 \end{cases}. \quad (5)$$

Thus, $\ell = \alpha a d_n$ for $R_2 \leq R_2^*$, where R_2^* is determined by the condition $ad_n/d = 1$. If $a > 1$ we get $R_2^* < 0$. This delay in the decrease of ℓ when R_2 becomes negative can also be seen in Fig. 12 of Ref. [3] for the axial spacing of vortices. We expect this crossover to be even a smooth process. Therefore we demand that the stability curve $R_1(R_2)$ is at least continuously differentiable. This will fix the parameters a and R_2^* . Coles uses the same ansatz $\ell = \alpha a d_n$ but for the whole range $R_2 \leq 0$ [14], which makes the stability boundary discontinuous at $R_2 = 0$.

Now we address the remaining question at which position r_p the virtual motion of the rings has to be considered. At first sight, one might think to choose it as to maximize the virtual energy gain. This leads to $r_p = r_1$. But more reasonable seems a position where the fluid is able to move in radial direction if instability indeed sets in. For Taylor vortices radial fluid motion is strongest near the gap center. This suggests choosing

$$r_p = r_1 + \frac{d}{2} \Delta(a \frac{d_n}{d}). \quad (6)$$

Experimental data [18] indicate that this might be reasonable also for flow patterns other than Taylor vortices.

Let us first evaluate the critical Reynolds number for resting outer cylinder defined as $R_{1,c} = R_1(R_2 = 0)$. For $R_2 = 0$ we have $r_n = r_2$, $\ell = \alpha d$ and $r_p = (r_1 + r_2)/2$, yielding from (4)

$$R_{1,c}(\eta) = \frac{1}{\alpha^2} \frac{(1+\eta)^2}{2\eta\sqrt{(1-\eta)(3+\eta)}}, \quad (7)$$

where all constant factors meant by ‘ \sim ’ have been absorbed in α . We fix α by matching $R_{1,c}(\eta)$ to linear stability theory in the narrow gap limit, because in this limit $R_{1,c}$ is known very accurately, e.g. [3,5,16]. The combination $4(1-\eta)R_{1,c}^2/(1+\eta) = T_c$ is the critical Taylor number for $R_2 = 0$ whose value for $\eta \rightarrow 1$ is $2/\alpha^4 = T_c \approx 3416$ [5]. Thus we have $\alpha = 0.1556$ corresponding to $\ell = d/6.427$, a reasonable value, which was also found by the same reasoning in [14].

Since $R_{1,c}$ diverges for $\eta \rightarrow 1$ and $\eta \rightarrow 0$, one better rescales R_1 and R_2 to discuss the stability curve $R_1(R_2)$ for general radius ratio η , cf also [6]. We employ $\mathcal{R}_1 = R_1/R_{1,c}$ and $\mathcal{R}_2 = R_2/(\eta R_{1,c})$, which will happen to be useful also in the limit when the Reynolds numbers go to infinity.

After eliminating $\alpha = \ell/d$ from (4) with (7) we arrive at the final formula for determining the stability boundary:

$$\left(\mathcal{R}_1 - \mathcal{R}_2 \right)^2 \frac{r_n^2 - r_p^2}{r_p^2} \frac{(1+\eta)^2}{(1-\eta)(3+\eta)} = \Delta(a \frac{d_n}{d})^{-4}. \quad (8)$$

We now calculate a as explained above and get

$$a(\eta) = (1-\eta) \left[\sqrt{\frac{(1+\eta)^3}{2(1+3\eta)}} - \eta \right]^{-1}. \quad (9)$$

a increases weakly with η from ≈ 1.4 to 1.6. We always took this $a(\eta)$, but differences to taking $a = const$ within this range could hardly be noticed in our following figures. Since ad_n can also be understood as the radial size of a Taylor vortex for counterrotating cylinders, this range of a can be confirmed by inspecting several figures in Refs. [3–5,8,9].

$$\mathcal{R}_2^*(\eta) = -\frac{\eta^2 + 4\eta + 1}{2(1+\eta)^2} \sqrt{\frac{3+\eta}{1+3\eta}} \quad (10)$$

is also weakly dependent on η , ranging between -0.75 and ≈ -0.90 . The continuous differentiability of the stability curve $\mathcal{R}_1(\mathcal{R}_2)$ at $ad_n/d = 1$ can not trivially be satisfied. But it is possible because Δ enters twice in (8), namely on the rhs. via ℓ , cf (4) and (5), and on the lhs. via r_p , cf (6). The argument of Δ is the same in both instances. The curvature of the boundary line has opposite sign to the left and to the right of \mathcal{R}_2^* for all η .

Eq. (8) together with (2), (5)–(7), and (9) constitute the main result of this work. It is an implicit equation determining the full stability curve $\mathcal{R}_1(\mathcal{R}_2)$ for all radius ratios η . It is easily solvable; analytically in special cases, and numerically in general.

Although we introduced several parameters, only α has been adjusted to linear stability theory. The others have been fixed by simple physical arguments and are not arbitrary fit parameters.

3. Comparison with data and stability theory

We now discuss the contents of (8), i.e., how the stability boundary globally looks like.

Fig. 1 shows $R_{1,c}(\eta)$, Eq. (7), compared with $R_{1,c}(\eta)$ from the Navier–Stokes linear stability theory and some selected experimental data. The good overall agreement for η approaching 1 and even for small η comes because Eq. (7) has the correct asymptotic behavior, cf [3,5] for $\eta \rightarrow 1$, [6] for $\eta \rightarrow 0$, and [9]. The $1/\eta$ law may be considered as a consequence of our choice for r_p , since with $r_p = r_1$ [15], for example, it is $R_{1,c} = \text{const}$ for $\eta \rightarrow 0$. Also the prefactor comes out remarkably well. We find $\eta R_{1,c} = 11.9$ in the limit $\eta \rightarrow 0$, whereas $\eta R_{1,c} \approx 11$ from linear stability theory [6], cf also the inset of Fig. 1. Some previous authors gave phenomenological scaling formulae which, however, do not show the correct exponents of the asymptotic laws for $\eta \rightarrow 0$ [19,14,12] or $\eta \rightarrow 1$ [12]. In particular, Coles finds $R_{1,c} \propto 1/(\eta\sqrt{\ln 1/\eta})$ for $\eta \rightarrow 0$ [14] which does not agree with linear stability theory (see the inset of Fig. 1 which clearly does not show a logarithmic singularity). The origin of this logarithmic singularity is that he took an integral mean of $-L^2(r)'/r^3$ over the range $r_1 \leq r \leq r_n$ for $R_2 < 0$, and $r_1 \leq r \leq r_2$ for $R_2 \geq 0$, respectively, instead of choosing a well-localized position r_p as we do.

In Figs. 2–4 the corresponding comparison is offered for the stability boundary (8), in the original variables $R_1(R_2)$, for $\eta = 0.20, 0.50$, and 0.964 , covering the whole range for which experimental data seem to be available. Intermediate values of η as in Refs. [3,11–13] give essentially the same satisfying picture.

For $R_2 \geq 0$ we find excellent quantitative agreement, and for $R_2 < 0$ there still is satisfactory agreement. The remaining discrepancies may be attributed to several reasons. First, the experimental data are affected by the finite length of the cylinders which becomes important for sufficiently negative R_2 [20,12]. This can be clearly seen in Fig. 3 as a deviation of the Donnelly–Fultz data from linear stability theory, the latter being calculated with aspect ratio infinity. Snyder’s data in Figs. 2 and 4 are supposed to be free of finite length effects [12]. Still, the difference of his data to our curve in Fig. 4 near $R_2 = 0$ is significantly larger than in other cases if we take the η value reported in [12], $\eta = 0.959$. But the deviation is much below the claimed 1% error in the experimental value for η [12]; we indicated the corresponding error in $R_{1,c}$ by a bar. Since the deviation could be caused by the strong η dependence $\sim 1/\sqrt{1-\eta}$, cf Fig. 1, we match the $R_{1,c}$ values of the experimental data and of the linear stability theory (and thus our Eq. (7)) by choosing $\eta = 0.964$. Now we find the same satisfactory overall picture as for the other η values.

Our curves correctly show a minimum at some negative R_2 . This can be attributed to the crossover in the boundary condition from solid to free. $a = 1$ leads to a

non-differentiable corner-type minimum at $R_2 = 0$ and to considerably higher curves for $R_1(R_2)$ at counterrotation, as was also found in [15]. Further on, taking $a > 1$ and $R_2^* = 0$ as in [14] gives a minimum at $R_2 = 0$ which is not even continuous.

It is not surprising that our minimum’s position

$$\mathcal{R}_{2,\min}(\eta) = -\frac{1-\eta}{2(1+\eta)}\sqrt{\frac{3+\eta}{1+3\eta}},$$

its depth and width do not match the measurements too well since the minimum is located in the crossover region $R_2^* \leq R_2 \leq 0$. We have marked R_2^* with an arrow in the figures. Choosing some other, smoother crossover function Δ in (5) allows to modify the location and the width of the minimum.

Interestingly, for $\eta \rightarrow 1$ the minimum is exactly at $R_2 = 0$, cf Fig. 4, independent of the value of a (as long as $a > 1$) and of the precise form of Δ , and nicely compatible with experiment [3,12] and theory [3,5,6,8,9].

For R_2 far left of the minimum our curves calculated from (8) are clearly systematically too high. Before discussing this, we complete our analysis by looking at interesting special cases, in which explicit formulae follow.

4. Asymptotic formulae

As long as the vortex flow fills the whole gap, i.e., for $\mathcal{R}_2 \geq \mathcal{R}_2^*$, we have $\Delta(ad_n/d) = 1$; then Eq. (8) can be solved for \mathcal{R}_1 :

$$\mathcal{R}_1 = \frac{1-\eta}{3+\eta}\mathcal{R}_2 + \sqrt{1 + \left(2\frac{1+\eta}{3+\eta}\mathcal{R}_2\right)^2}, \quad (11)$$

for $\mathcal{R}_2 \geq \mathcal{R}_2^*$.

This implies a leading correction $\propto \mathcal{R}_2^{-2}$ relative to the Rayleigh line $\mathcal{R}_1 = \mathcal{R}_2$ for large \mathcal{R}_2 .

For $\mathcal{R}_2 < \mathcal{R}_2^*$, the quantity

$$\varepsilon = \left(\frac{r_n}{r_1}\right)^2 - 1 = \frac{1-\eta^2}{\eta^2} \frac{\mathcal{R}_1}{\mathcal{R}_1 - \mathcal{R}_2} \quad (12)$$

is a suitable parameter for discussing the strongly counterrotating case as well as the narrow and wide gap limits. For $\varepsilon \rightarrow 0$, corresponding to $r_n \rightarrow r_1$, we find from (8)

$$-\eta^2\mathcal{R}_2 = \left(\frac{\mathcal{R}_1}{C}\right)^{5/3} - \eta^2\mathcal{R}_1, \quad \mathcal{R}_1 \gg (1-\eta^2)^{3/2}C^{5/2}, \quad (13)$$

$$C(\eta) = \left(\frac{2^5(3+\eta)}{a^4(2-a)(1+\eta)^7}\right)^{1/5}.$$

The leading term for large $|\mathcal{R}_2|$ reads

$$\mathcal{R}_1 = C(\eta)|\eta^2\mathcal{R}_2|^{3/5}, \quad \mathcal{R}_2 \rightarrow -\infty. \quad (14)$$

The exponent $3/5$ was already found by Donnelly and Fultz [10] by a dimensional argument. That, of course,

did not yet give the complete η dependent prefactor $\eta^{6/5}C(\eta)$ and also not the non-trivial corrections contained in (13). These turn out to be non-negligible in the range of \mathcal{R}_2 accessible to experiment. Since $\varepsilon \propto |\eta^2 \mathcal{R}_2|^{-2/5}$ for sufficiently large $|\eta^2 \mathcal{R}_2|$, the convergence to the leading behavior (13) and (14) is rather bad in terms of \mathcal{R}_2 for fixed η and becomes worse with decreasing η .

Coles [14] has chosen the value of a by matching his analytic formula to linear stability theory for $\eta \rightarrow 1$ in the limit $R_2 \rightarrow -\infty$. This choice leads to an η independent value of $a \approx 1.3$. This means he adjusted his formula to two values from linear stability theory whereas we only use one.

On the other hand, for $\eta \rightarrow 1$ Eq. (13) becomes exact for all $\mathcal{R}_2 \leq \mathcal{R}_2^*$. In this limit we have $\mathcal{R}_2^* = -3/4$ and $a = 8/5$ from (10) and (9). Furthermore, the position of the minimum approaches $\mathcal{R}_{2,\min} = 0$, and the stability boundary becomes symmetric for $|\mathcal{R}_2| \leq |\mathcal{R}_2^*|$, cf Fig. 4.

Therefore, in Fig. 4 the asymptotic formula (13) would be indistinguishable from the full curve, whereas in Figs. 2 and 3 it would be a rather poor approximation.

Of particular interest is the wide gap limit $\eta \rightarrow 0$, since it has not yet been examined very much. It is accompanied by large ε for any finite \mathcal{R}_2 interval, cf (12). For $\varepsilon \rightarrow \infty$ the relevant expansion parameter in (8) is $\varepsilon^{-1/2}$. We keep the two leading terms and consider η small in them:

$$\mathcal{R}_1 = \frac{1}{2}\sqrt{3} + \frac{3+2\sqrt{2}}{1+\sqrt{2}}\eta\sqrt{1-\frac{2}{\sqrt{3}}\mathcal{R}_2}, \quad (15)$$

for $-\mathcal{R}_1/\eta^2 \ll \mathcal{R}_2 \leq \mathcal{R}_2^*$.

Here $\mathcal{R}_2^* = -\sqrt{3}/2$ and $a = \sqrt{2}$ for $\eta \ll 1$, cf (10) and (9). Because of the bad convergence in terms of $\varepsilon^{-1/2}$ to this limiting behavior the line $\mathcal{R}_1(\mathcal{R}_2)$ according to (15) is clearly visible only for $\eta \lesssim 0.01$. Of course, for fixed $\eta > 0$ and sufficiently largely negative \mathcal{R}_2 equation (13) is valid again because then $\varepsilon \rightarrow 0$ instead of $\rightarrow \infty$. As can be seen from (14) and (15) the most reasonable variables for strongly counterrotating cylinders, i.e., $\mathcal{R}_2 \rightarrow -\infty$, are \mathcal{R}_1 and $\eta^2 \mathcal{R}_2$. Note that the meaning of their ratio is $\eta^2 \mathcal{R}_2 / \mathcal{R}_1 = \omega_2 / \omega_1$. This frequency ratio as a parameter has already been used in [3,5].

5. Improvements

Now we discuss possible corrections to our main result. It turns out that the precise value of r_p has a surprisingly well observable influence on the stability curve.

To see this, we generalize (6) to

$$r_p = r_1 + p d \Delta(a \frac{d_n}{d}) \quad (16)$$

with the new parameter p describing the position of the disturbance; $p = 1/2$ gives the previous case, cf (6), to locate it in the center of the relevant gap.

Treating p as a free fit parameter we find the remaining discrepancies between our stability boundary and that of experiment or linear stability calculations nearly removed for $p = 0.47, 0.46, 0.43$, corresponding to $\eta = 0.964, 0.5, 0.2$, respectively. This is exemplified in Fig. 2 by the dotted line; for the other η values the agreement is similarly good. Position shifts of this magnitude are confirmed by several figures in Refs. [3,5,8,9] which show that the center of each Taylor vortex is situated nearer towards the inner cylinder. Analytically we find roughly $a \sim 1/p$ and C approximately $\sim p$ if p is near $1/2$ and for η not too small. We could not figure out a simple physical condition for fixing $p(\eta)$. For example, second order continuous differentiability of the stability boundary at \mathcal{R}_2^* turns out not to be realizable.

Our argument does not take into consideration non-axisymmetric perturbations of the laminar flow. As we know from experiment [18] and linear stability theory [8], the relevant perturbations are indeed non-axisymmetric beyond a finite negative R_2 . They lead to a somewhat lower stability boundary than that determined with axisymmetric disturbances. The difference for the values of R_2 considered here is pretty small. It turns out that our deviations from the correct stability boundary are of the same order of magnitude. Furthermore these deviations start already near $R_{2,\min}$. We therefore think it to be acceptable that the possibility of non-axisymmetric disturbances is neglected.

Of course, also other corrections have to be considered. For example, energy dissipation is curvature dependent. Therefore it seems natural to extend the rhs. of (3) to $(\nu^2/\ell^4)(\delta r)^2(1 + b\ell/r_p)$ with b a constant. ℓ/r_p vanishes for $\eta \rightarrow 1$ or for $\mathcal{R}_2 \rightarrow -\infty$ and is rather small even for $\eta \rightarrow 0$; for example in the case $\mathcal{R}_2 = 0$ we have $\ell/r_p = \alpha \approx 0.16$. Thus (13) remains valid, but with a different a in C . Note, without this curvature correction the value for $a(\eta)$, Eq. (9), is close to $a = 8/5$ which minimizes C for fixed η but variable a . In general, this means the curvature correction shifts the stability boundary upwards if \mathcal{R}_2 is well below \mathcal{R}_2^* counteracting the influence of the r_p shift.

6. Summary

Similar arguments as are presented here for Taylor–Couette flow have been invoked to elucidate the physical mechanism of the Rayleigh–Bénard instability [21]. But in the Taylor–Couette system it carries much further since this has two additional parameters, η and R_2 , whose influence on the shape of the stability boundary we could successfully explain. At Rayleigh–Bénard instability a corresponds to the ratio of the α 's for the two distinct cases of free and solid boundary conditions. From [5] we find for this ratio ≈ 1.13 . We understand this value closer to 1 than we found here for the counterrotating Taylor–Couette system from the stronger influence of the surface tension in an open Rayleigh–Bénard system in

contrast to the completely missing surface tension at the nodal surface r_n in Taylor–Couette flow. Therefore this nodal surface is much softer, allowing for a larger extension of the Taylor vortices beyond r_n . One could check this by putting another fluid layer on top of the original Rayleigh–Bénard fluid; if this diminishes the surface tension, a larger a should result.

To conclude: While accurate results for the onset of the Taylor–Couette instability derived by linear stability theory are available, in this paper we have drawn a picture that gives comprehensive physical insight into the instability mechanism and yields simple analytical expressions for the stability boundary in the full parameter space. These agree astonishingly well with experimental data and with the rigorous theory, especially in regard of how straightforward the argument is. The position where the initial perturbation occurs and the change of the type of boundary when the nodal surface moves inwards turned out to be important for the wide gap behavior and for the existence of a minimum of the stability boundary for negative R_2 . The values found for the parameters α and a are reasonable and agree with experiment as well. Assuming a radius ratio dependent small shift of the perturbation’s initial position towards the inner cylinder we were able to understand the remaining quantitative discrepancies.

We believe that these simple ideas should be applicable to instabilities in more complicated rotating fluid flows, where the standard linear stability analysis is too difficult.

Acknowledgments: We thank Thomas Gebhardt and Martin Holthaus for their interest and help. S. G. acknowledges stimulating discussions about similar analysis of thermal convection with Stefan Thomae, quite some time ago, during a sabbatical stay at the Max-Planck-Institut für Mathematik in Bonn.

[1] M. M. Couette, “Sur un nouvel appareil pour l’étude du frottement des fluids”, *Comptes Rendus* **107**, 388–390 (1888).
[2] A. Mallock, “Determination of the viscosity of water”, *Proc. Roy. Soc. (London)* **A 45**, 126–132 (1888).
[3] G. I. Taylor, “Stability of a viscous liquid contained between two rotating cylinders”, *Phil. Trans. Roy. Soc. London* **A 223**, 289–343 (1923).
[4] R. Tagg, “The Couette–Taylor problem”, *Nonlin. Science Today* **4**, 1–25 (1994).
[5] S. Chandrasekhar, *Hydrodynamic and Hydromagnetic Instability*, 1st ed. (Clarendon Press, Oxford, 1961).
[6] J. Walowit, S. Tsao, and R. C. DiPrima, “Stability of flow between arbitrarily spaced concentric cylindrical surfaces including the effect of a radial temperature gradient”, *J. Appl. Mech.* **31**, 585–593 (1964).

[7] D. D. Joseph, *Stability of Fluid Motions I*, 1st ed. (Springer-Verlag, Berlin Heidelberg, 1976).
[8] P. G. Drazin and W. H. Reid, *Hydrodynamic Stability*, 1st ed. (Cambridge University Press, Cambridge, 1981).
[9] T. Gebhardt and S. Grossmann, “The Taylor–Couette eigenvalue problem with independently rotating cylinders”, *Z. Phys.* **B 90**, 475–490 (1993).
[10] R. J. Donnelly and D. Fultz, “Experiments on the stability of viscous flow between rotating cylinders. II. Visual observations”, *Proc. Roy. Soc. (London)* **A 258**, 101–123 (1960).
[11] D. Coles, “Transition in circular Couette flow”, *J. Fluid Mech.* **21**, 385–425 (1965).
[12] H. A. Snyder, “Stability of rotating Couette flow. II. Comparison with numerical results”, *Phys. Fl.* **11**, 1599–1605 (1968).
[13] C. D. Andereck, S. S. Liu, and H. L. Swinney, “Flow regimes in a circular Couette system with independently rotating cylinders”, *J. Fluid Mech.* **164**, 155–183 (1986).
[14] D. Coles, “A note on Taylor instability in circular Couette flow”, *J. Appl. Mech.* **34**, 529–534 (1967).
[15] B. Eckhardt and D. Yao, “Local stability analysis along Lagrangian paths”, *Chaos, Solitons and Fractals* (1995), in press.
[16] L. D. Landau and E. M. Lifschitz, *Fluid Mechanics*, vol. VI of *Course of Theoretical Physics*, 2nd ed. (Pergamon Press, Oxford, 1987).
[17] Lord Rayleigh, “On the dynamics of revolving fluids”, *Proc. Roy. Soc. (London)* **A 93**, 148–154 (1916).
[18] H. A. Snyder, “Waveforms in rotating Couette flow”, *Int. J. Non-Linear Mech.* **5**, 659–685 (1970).
[19] L. Prandtl, *Abriss der Strömungslehre*, 1st ed. (Vieweg, Braunschweig, 1931), *Essentials of Fluid Dynamics* (Stechert-Hafner, New York, 1952).
[20] H. A. Snyder, “Stability of rotating Couette flow. I. Asymmetric waveforms”, *Phys. Fl.* **11**, 728–734 (1968).
[21] C. Normand, Y. Pomeau, and M. G. Velarde, “Convective instability: A physicist’s approach”, *Rev. Mod. Phys.* **49**, 581–624 (1977).
[22] T. Gebhardt, private communication.

FIG. 1. Critical Reynolds number $R_{1,c}$ as a function of η from Eq. (7) (solid line), from linear stability theory [9] (dashed line), and from various experiments [3,10–13] (symbols). For the error bar see Fig. 4. Inset: The same for $R_{1,c}$ rescaled to $R_{1,c} \eta \sqrt{1-\eta}$.

FIG. 2. The stability line $R_1(R_2)$ for $\eta = 0.2$ from Eq. (8) (solid line), and from experiment [12] (symbols). The dotted line is our result with the perturbation’s position parameter set to $p = 0.43$, see Eq. (16). The arrow marks R_2^* . Inset: The same on a magnified scale.

FIG. 3. The stability line $R_1(R_2)$ for $\eta = 0.5$ from Eq. (8) (solid line), from linear stability theory [9,22] (dashed line), and from experiment [10] (symbols). The dashed line may be reproduced with $p = 0.46$. The arrow marks R_2^* . Inset: The same on a magnified scale.

FIG. 4. The stability line $R_1(R_2)$ for $\eta = 0.964$ from Eq. (8) (solid line), and from experiment [12] (symbols). The vertical bar denotes the error in $R_{1,c}$ due to $\eta = 0.959 \pm 1\%$ [12]. $p = 0.47$ fits the experimental data. The arrow marks R_2^* . Inset: The same on a magnified scale.

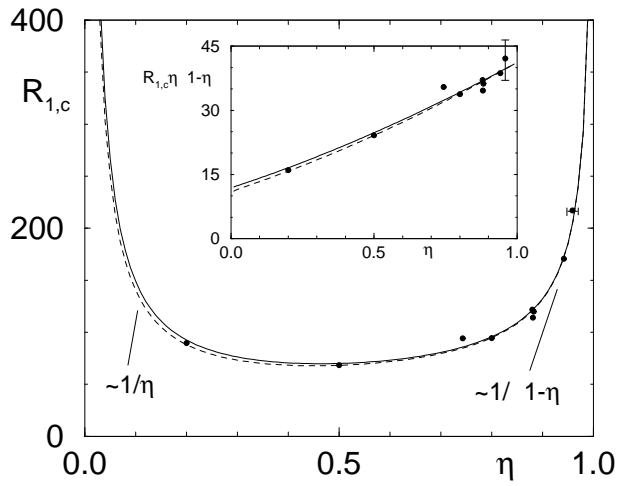


Figure 1

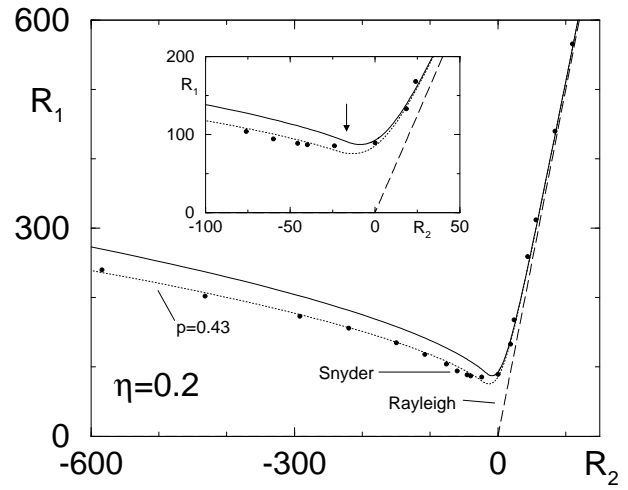


Figure 2

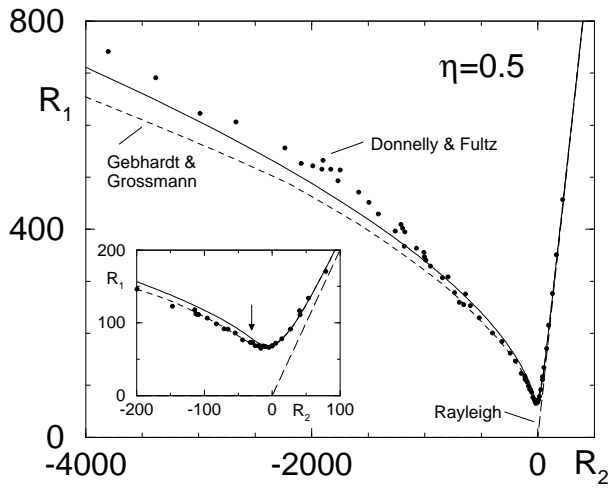


Figure 3

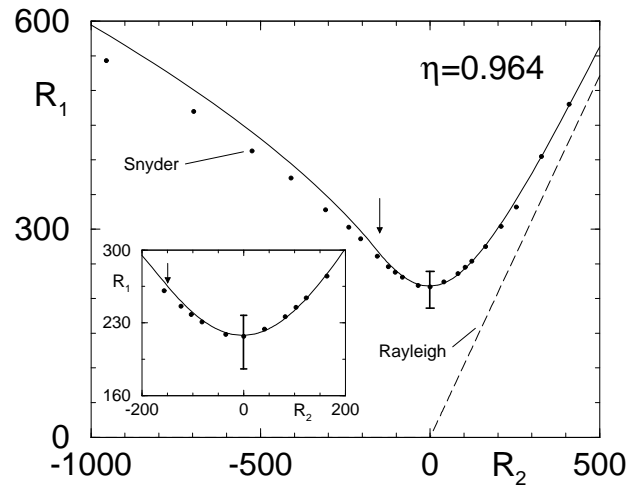


Figure 4